J. Plasma Phys. (2017), *vol.* 83, 725830603
doi:10.1017/S0022377817000952

Electron energy and vibrational distribution functions of carbon monoxide in nanosecond atmospheric discharges and microsecond afterglows

L. D. Pietanza[1],†, G. Colonna[1] and M. Capitelli[1]

[1]CNR Nanotec, P.Las.M.I Lab, via Amendola 122/D, 70126 Bari, Italy

(Received 15 September 2017; revised 24 November 2017; accepted 27 November 2017)

Nanopulse atmospheric carbon monoxide discharges and corresponding afterglows have been investigated in a wide range of applied reduced electric field ($130 < E/N < 200$ Td) and different pulse durations (2–50 ns). The results have been obtained by solving an appropriate Boltzmann equation for the electron energy distribution function (EEDF) coupled to the kinetics of vibrational and electronic excited states as well as to a simplified plasma chemistry for the different species formed during the activation of CO. The molar fraction of electronically excited states generated in the discharge is sufficient to create structures in the EEDF in the afterglow regime. On the other hand, only for long duration pulses (i.e. 50 ns), non-equilibrium vibrational distributions can be observed especially in the afterglow. The trend of the results for the case study $E/N = 200$ Td, $\tau_{pulse} = 2$ ns is qualitatively and quantitatively similar to the corresponding case for CO_2 implying that the activation of CO_2 by cold plasmas should take into account the kinetics of formed CO with the same accuracy as the CO_2 itself.

Key words: electric discharges, plasma chemical reactions, plasma simulation

1. Introduction

Much attention is being devoted to high pressure non-equilibrium plasmas due to their importance for many technological applications. In particular, nanopulse atmospheric discharges are widely investigated either in the one pulse modality or in repetitive nanopulsed discharges. The experimental characterization of one pulse and multipulse discharges is well developed mostly due to the their relatively easy realization.

The chemical kinetics either in the discharge or in the post-discharge is usually decoupled from the electron component, a hypothesis which can be open to question especially in the post-discharge regime. Vibrational–chemical modelling of CO and mixtures of CO_2/CO molecules have been developed for aerospace applications not considering the electron induced processes (see Kosareva & Nagnibeda 2017; Mishina & Kustova 2017).

† Email address for correspondence: luciadaniela.pietanza@cnr.it

The coupling between EEDF and excited state kinetics has a long history as can be appreciated by looking at different reviews and monographies on the subject (Cacciatore *et al.* 1986; Capitelli *et al.* 2000, 2016) in general dealing with moderate pressure conditions (Torr regime).

High pressure nanosecond pulse discharges followed by a long afterglow have been investigated for nitrogen, emphasizing the dependence of the electron energy distribution function on the concentrations of electronically excited states. Indeed, superelastic electronic collisions of cold electrons with metastable states were responsible of the formation of structures in EEDF (Gorse *et al.* 1986; Colonna *et al.* 2015). In these studies, vibrationally excited molecules play a minor role in affecting the plasma kinetics due to the fact that the short pulse considered is unable to create a large concentration of vibrationally excited states. The situation changes when modulating the duration of the pulse as well as the time between one pulse and the next as recently shown in the case of atmospheric hydrogen plasmas (Colonna *et al.* 2015; Colonna, D'Ammando & Pietanza 2017*a*).

Very recently, nanosecond discharges were also studied for the CO_2 system for conditions similar to those occurring in dielectric barrier discharges (DBD) (Capitelli *et al.* 2017*a*).

In the present paper, we consider one pulse nanosecond discharge and corresponding afterglow in reacting CO. The choice of CO is justified by the importance of this system in different applications including the infrared CO laser as well as the possibility of creating micro and nano carbon materials when the corresponding discharge produces a long plateaux in the vibrational distribution function (Mori & Suzuki 2009; Belov *et al.* 2017). Moreover, the kinetics of CO under non-equilibrium plasma conditions is of primary importance in CO_2 discharges when the dissociation of CO_2 produces important quantities of CO. This problem, largely underestimated by the recent efforts in the activation of CO_2 by cold plasmas (Kozak & Bogaerts 2014, 2015; Pietanza *et al.* 2015; Bogaerts *et al.* 2016; Pietanza *et al.* 2017*a*), can be solved by inserting in the CO_2 system a robust plasma kinetics describing the CO reacting system.

The state to state plasma kinetics of CO has been recently re-examined (see Pietanza, Colonna & Capitelli 2017*b*) for conditions typical of moderate pressure microwave discharges, taking into account the efforts made in the past by Gorse, Cacciatore & Capitelli (1984*a*), Gorse & Capitelli (1984*b*).

The new model contains several important improvements with respect to the past attempts either in the quality of cross-sections of elementary processes or in the plasma kinetic model describing the activation of CO. In particular, the electron-impact resonant vibration excitation processes in CO (the electron–vibration (e–V) processes) are nowadays well described thanks to the large effort made by Laporta *et al.* (2012), Laporta, Tennyson & Celiberto (2016). These new data can be used instead of the assumption of e–V linking only the first 10 CO vibrational levels Gorse, Cacciatore & Capitelli 1984*a*; Gorse & Capitelli 1984*b*. These processes can be important for very short pulses when the e–V collisions from $v = 0$ dominate other processes in the formation of the vibrational distribution function of CO. Another important improvement is the new activation energy value of the Boudouard reactions, i.e. $E_a = 8.3$ eV calculated by Barreto *et al.* (2017), instead of 6 eV used in Gorse, Cacciatore & Capitelli 1984*a*; Gorse & Capitelli 1984*b* and 11.3 eV in Essenhigh *et al.* (2006), which affects either the formation of CO_2 in pure CO discharges or the deactivation of the plateau in the vibrational distribution of CO.

On the other hand, the present kinetic model considers the presence of metastable excited states of CO and corresponding C and O atoms produced in the discharge,

https://doi.org/10.1017/S0022377817000952 Published online by Cambridge University Press

which are able to form a large number of structures in the EEDF in the post-discharge regime as a result of superelastic electronic collisions, not considered in Gorse & Capitelli (1984*a*,*b*).

The paper is divided into 4 sections. After the introduction, § 2 describes the model, § 3 reports the results obtained by changing the initial conditions of the discharge, § 4 reports conclusions and perspectives. Explicit expressions of the dissociation rates are reported in an appendix A at the end of the paper.

2. The model

The model is based on the solution of a zero-dimensional time dependent Boltzmann equation for the electrons coupled to the non-equilibrium vibrational and electronic excited state kinetics of the CO molecule with a simple dissociation and ionization kinetics describing the plasma mixture (Capitelli *et al.* 2017*a*,*b*; Pietanza *et al.* 2017*c*).

The electron Boltzmann equation is coupled in this case to the non-equilibrium vibrational kinetics of the CO levels, to the kinetics of electronically excited states of CO, C and O species, to the dissociation–recombination kinetics, to the ionization–recombination kinetics. All the kinetics are self-consistently solved in a time dependent manner.

The electron Boltzmann equation can be written in the following compact form

$$\frac{\mathrm{d}n(\varepsilon, t)}{\mathrm{d}t} = -\frac{\mathrm{d}J_E}{\mathrm{d}\varepsilon} - \frac{\mathrm{d}J_{\mathrm{el}}}{\mathrm{d}\varepsilon} - \frac{\mathrm{d}J_{\mathrm{e\text{–}e}}}{\mathrm{d}\varepsilon} + S_{\mathrm{in}} + S_{\mathrm{sup}}, \tag{2.1}$$

where $n(\varepsilon, t)$ represents the number of electrons in the energy range ε to $\varepsilon + \mathrm{d}\varepsilon$, linked to the EEDF $f(\varepsilon, t)$ by

$$f(\varepsilon, t) = \frac{n(\epsilon, t)}{N_e(t)}\varepsilon^{-1/2}, \tag{2.2}$$

with the normalization condition

$$N_e(t) = \int_0^\infty n(\varepsilon, t)\,\mathrm{d}\varepsilon, \quad \int_0^\infty f(\varepsilon, t)\,\mathrm{d}\varepsilon = 1, \tag{2.3a,b}$$

where $N_e(t)$ is the instantaneous electron number density.

The first three terms on the right-hand side of (2.1) correspond to fluxes J along the electron energy axis due to, respectively, the electric field $\mathrm{d}J_E/\mathrm{d}\varepsilon$, the elastic electron–molecule collisions $\mathrm{d}J_{\mathrm{el}}/\mathrm{d}\varepsilon$ and the electron–electron (e–e) collisions $\mathrm{d}J_{\mathrm{e\text{–}e}}/\mathrm{d}\varepsilon$. The sources terms S are due to inelastic collisions including electronic excitation, dissociation and ionization processes S_{in}, while the last term S_{sup} denotes superelastic collisions involving electrons and vibrationally and electronically excited states.

Explicit expressions of the different terms in (2.1) can be found in a number of papers (Rockwood 1973; Capitelli *et al.* 2016).

The plasma mixture considered is composed of the following species: CO, CO_2, C, O, CO^+, CO_2^+, C^+, O^+ and e^-.

The energy level diagrams of CO, C and O are schematically represented in figure 1. The CO molecule has 80 vibrational levels in the ground electronic state ($X^1\Sigma^+$), whose energies, calculated in the anharmonic oscillator approximation, have been taken from the work of Laporta *et al.* (2016), together with the dissociation energy value of 11.128 eV ($CO \rightarrow C(^3P) + O(^3P)$). Several singlet and triplet CO electronic excited states have been considered, in particular, three triplet states, $a^3\Pi$ (6.006 eV), $a'^3\Sigma^+$ (6.863), $b^3\Sigma^+$ (10.40 eV) and four singlet states, $A^1\Pi$ (8.03 eV), $B^1\Sigma^+$ (10.78 eV), $C^1\Sigma^+$ (11.40 eV), $E^1\Sigma^+$ (11.52 eV).

https://doi.org/10.1017/S0022377817000952 Published online by Cambridge University Press

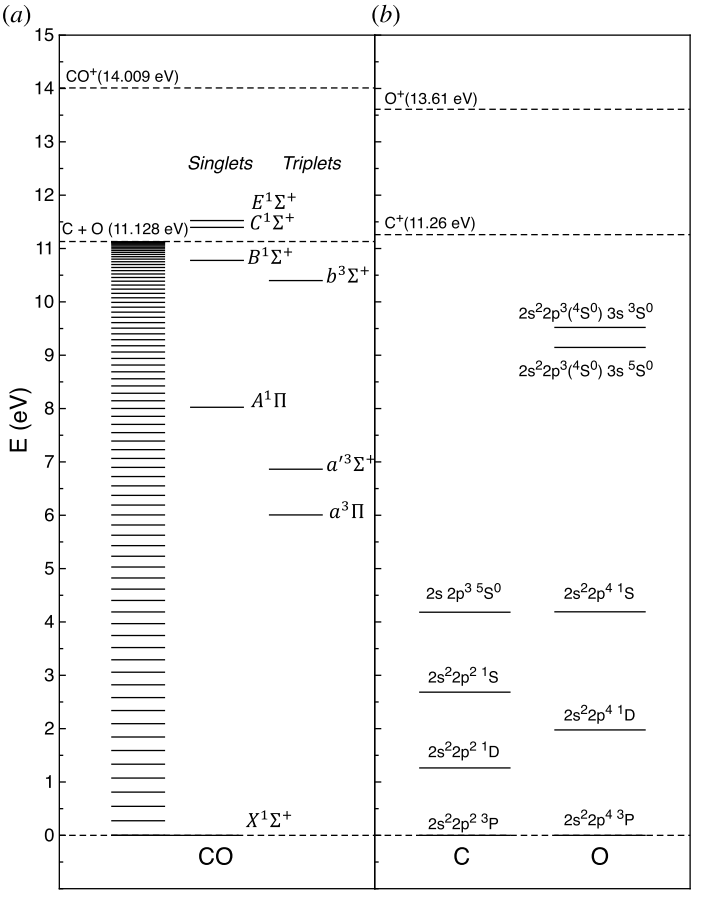

FIGURE 1. Schematic representation of the (*a*) CO and (*b*) C and O energy level diagrams.

For C and O atoms, only four and five electronic levels are accounted for, see figure 1(*b*), which from now on will be labelled as C(^{3}P), C(^{1}D), C(^{1}S), C(^{5}S^0) and O(^{3}P), O(^{1}D), O(^{1}S), O(^{3}S) and O(^{5}S), respectively. Their energies have been taken from the National Institute of Standards and Technology (NIST) Atomic Spectra Database.

The electron-impact cross-sections entering in the Boltzmann equation are those corresponding to the processes listed in table 1, together with the corresponding sources and discussed in a recent paper on the application of the model to microwave plasmas and afterglows (Pietanza *et al.* 2017*b*). The most important improvement with respect to the current literature is a complete set of electron-impact resonant vibration excitation cross-sections linking all the vibrational levels of CO (see processes e–V_{Res} in table 1) as well as the consideration of the resonant dissociation cross-sections depending on the vibrational levels of CO (see process $D_{Res}(v)$ in table 1).

2.1. *CO plasma chemistry*

In the model, the following two reactive channels assisted by vibrational excitation (pure vibrational mechanisms, PVM) are accounted for:

https://doi.org/10.1017/S0022377817000952 Published online by Cambridge University Press

Process	Label	Reference
$e + X \leftrightarrow e + X$, $X = \mathrm{CO}$, $\mathrm{CO_2}$, C, O, $\mathrm{CO^+}$, $\mathrm{C^+}$, $\mathrm{O^+}$	MT	Gorse & Capitelli 1984*b*; Pitchford *et al.* 2017
$e + \mathrm{CO}(0) \leftrightarrow e + \mathrm{CO^+} + e$	$\mathrm{I_{CO}}(0)$	Itikawa 2015
$e + \mathrm{CO}(v) \leftrightarrow e + \mathrm{CO^+} + e$	$\mathrm{I_{CO}}(\mathrm{v})$	Itikawa 2015
$e + \mathrm{CO}(0) \leftrightarrow e + \mathrm{CO}(X)$, $X = a^3\Pi$, $a'^3\Sigma^+$, $b^3\Sigma^+$, $A^1\Pi$, $B^1\Sigma^+$, $C^1\Sigma^+$, $E^1\Sigma^+$	$\mathrm{Met_{CO}}$	Itikawa 2015
$e + \mathrm{CO}(0) \leftrightarrow e + \mathrm{C} + \mathrm{O}$	$\mathrm{D_{dir}}(0)$	Cosby 1993
$e + \mathrm{CO}(v) \leftrightarrow e + \mathrm{C} + \mathrm{O}$	$\mathrm{D_{dir}}(\mathrm{v})$	Cosby 1993; Fridman 2008
$e + \mathrm{CO}(v_i) \rightarrow \mathrm{CO^-}(^2\Pi) \rightarrow e + \mathrm{CO}(v_f)$	$\mathrm{e\text{–}V_{Res}}$	Laporta *et al.* 2012
$e + \mathrm{CO}(v) \rightarrow \mathrm{CO^-}(^2\Pi) \rightarrow e + \mathrm{C}(^3P) + \mathrm{O}(^3\mathrm{P})$	$\mathrm{D_{Res}}(\mathrm{v})$	Laporta *et al.* 2016
$e + \mathrm{C}(^3\mathrm{P}) \leftrightarrow e + \mathrm{C^+}$	$\mathrm{I_C}$	Wang, Zatsarinny & Bartschat 2013
$e + \mathrm{O}(^3\mathrm{P}) \leftrightarrow e + \mathrm{O^+}$	$\mathrm{I_O}$	Laher & Gilmor 2016
$e + \mathrm{C}(^3\mathrm{P}) \leftrightarrow e + \mathrm{C}(X)$, $X = {}^1\mathrm{D}$, ${}^1\mathrm{S}$, ${}^5\mathrm{S^0}$	e–C	Wang *et al.* 2013
$e + \mathrm{O}(^3\mathrm{P}) \leftrightarrow e + \mathrm{O}(X)$, $X = {}^1\mathrm{D}$, ${}^1\mathrm{S}$, ${}^3\mathrm{S^0}$, ${}^5\mathrm{S^0}$	e–O	Laher & Gilmor 2016

TABLE 1. Electron-impact processes: momentum transfer (MT), ionization (I), excitation and deexcitation of CO electronically excited states, assumed as metastable states (Met), dissociation (D), vibrational excitation (e–V), excitation and deexcitation of C and O excited states (e–C, e–O).

(1) direct dissociation ($\mathrm{PVM_1}$)

$$\mathrm{CO}(v) + M \rightarrow \mathrm{C} + \mathrm{O} + \mathrm{M}. \tag{2.1.1}$$

(2) Boudouard or disproportionation reaction ($\mathrm{PVM_2}$)

$$\mathrm{CO}(v) + \mathrm{CO}(w) \rightarrow \mathrm{CO_2} + \mathrm{C}. \tag{2.1.2}$$

The equation for the $\mathrm{PVM_1}$ and $\mathrm{PVM_2}$ rate coefficients, can be found in the appendix A and have been derived from Essenhigh *et al.* (2006) and Pietanza *et al.* (2017*b*). The activation energy of process (2.1.2) has been considered equal to 8.3 eV from the work of Barreto *et al.* (2017).

The two PVM mechanisms can have an important role especially in microwave (MW) discharge and post-discharge conditions, while in nanopulse atmospheric discharges, dissociation occurs mainly through direct electron-impact mechanisms (DEM) as will be discussed in the present work (see also Capitelli *et al.* 2017*a*), i.e. through the following process

$$e + \mathrm{CO}(v) \leftrightarrow e + \mathrm{C} + \mathrm{O}. \tag{2.1.3}$$

Electron-impact ionization of CO, C and O is also considered, i.e.

$$e + \mathrm{CO}(v) \leftrightarrow e + \mathrm{CO^+} + e \tag{2.1.4}$$

$$e + \mathrm{C}(^3\mathrm{P}) \leftrightarrow e + \mathrm{C^+} \tag{2.1.5}$$

$$e + \mathrm{O}(^3\mathrm{P}) \leftrightarrow e + \mathrm{O^+}. \tag{2.1.6}$$

https://doi.org/10.1017/S0022377817000952 Published online by Cambridge University Press

The electron-impact rates of processes (2.1.3)–(2.1.6) are calculated from the corresponding cross-sections $\sigma(\varepsilon)$, used for the Boltzmann equation, the EEDF $f(\varepsilon)$ and the electron velocity $v(\varepsilon)$ by integrating over the electron energy ε

$$K = \int_{E_t} v(\varepsilon)\sigma(\varepsilon)f(\varepsilon)\,\mathrm{d}\varepsilon. \tag{2.1.7}$$

The formed C and O atoms, produced through both the PVM (see (2.1.1)) and DEM (see (2.1.3)) dissociation mechanisms, are allowed to recombine according to the process

$$\mathrm{C} + \mathrm{O} + \mathrm{M} \rightarrow \mathrm{CO} + \mathrm{M}. \tag{2.1.8}$$

Finally, CO^+ losses occur mainly by the dissociative recombination process

$$\mathrm{CO}^+ + e \rightarrow \mathrm{C} + \mathrm{O}. \tag{2.1.9}$$

The rate of processes (2.1.8) and (2.1.9) are taken from Kozak & Bogaerts (2014).

2.2. *CO vibrational kinetics*

The CO vibrational distribution function (VDF) is obtained by the solution of a coupled system of differential equations, one equation for each vibrational level, of the kind

$$\begin{aligned}\frac{\mathrm{d}N_v}{\mathrm{d}t} = &\left(\frac{\mathrm{d}N_v}{\mathrm{d}t}\right)_{\mathrm{e\text{–}V}} + \left(\frac{\mathrm{d}N_v}{\mathrm{d}t}\right)_{\mathrm{e\text{–}D}} + \left(\frac{\mathrm{d}N_v}{\mathrm{d}t}\right)_{\mathrm{e\text{–}I}} + \left(\frac{\mathrm{d}N_v}{\mathrm{d}t}\right)_{\mathrm{PVM}} \\ &+ \left(\frac{\mathrm{d}N_v}{\mathrm{d}t}\right)_{\mathrm{V\text{–}V}} + \left(\frac{\mathrm{d}N_v}{\mathrm{d}t}\right)_{\mathrm{V\text{–}T}} + \left(\frac{\mathrm{d}N_v}{\mathrm{d}t}\right)_{\mathrm{SE}},\end{aligned} \tag{2.2.1}$$

where e–V, e–D and e–I contributions correspond, respectively, to the electron-impact resonant vibrational excitation processes ($\mathrm{e\text{–}V_{Res}}$), to the two contributions of direct ($\mathrm{D_{Dir}}$) and resonant ($\mathrm{D_{Res}}$) dissociation processes and to ionization ($\mathrm{I_{CO}}$) processes listed in table 1. The PVM term corresponds to the contribution of dissociation induced by vibrational excitation due to both direct dissociation (2.1.1) and the Boudouard process (2.1.2). The last terms (V–V, V–T and SE) correspond to the following energy-exchange processes:

(1) V–V (vibration–vibration)

$$\mathrm{CO}(v) + \mathrm{CO}(w) \leftrightarrow \mathrm{CO}(v-1) + \mathrm{CO}(w+1) + \Delta\varepsilon. \tag{2.2.2}$$

(2) V–T (vibration–translation) by CO

$$\mathrm{CO}(v) + \mathrm{CO} \leftrightarrow \mathrm{CO}(v-1) + \mathrm{CO} + \Delta\varepsilon_T. \tag{2.2.3}$$

(3) V–T by C, O

$$\mathrm{CO}(v) + \mathrm{C} \leftrightarrow \mathrm{CO}(v-1) + \mathrm{C} + \Delta\varepsilon_T \tag{2.2.4}$$

$$\mathrm{CO}(v) + \mathrm{O} \leftrightarrow \mathrm{CO}(v-1) + \mathrm{O} + \Delta\varepsilon_T. \tag{2.2.5}$$

(4) SE (spontaneous emission)

$$\mathrm{CO}(v) \leftrightarrow \mathrm{CO}(w) + h\nu_{vw}. \tag{2.2.6}$$

The different rate coefficients are discussed by Pietanza *et al.* (2017*b*).

https://doi.org/10.1017/S0022377817000952 Published online by Cambridge University Press

$\tau_{EEDF} = (n_{CO}K_{eV}^{1,0})^{-1}$	$\tau_{e-V} = (n_e K_{eV}^{1,0})^{-1}$	$\tau_{V-V} = (n_{CO}K_{1,0}^{1,0})^{-1}$	$\tau_{V-T(CO)} = (n_{CO}K_{vT(CO)}^{1,0})^{-1}$	$\tau_{V-T(C,O)} = (n_C K_{vT(C,O)}^{1,0})^{-1}$
4.80×10^{-12} s	3.22×10^{-7} s	4.37×10^{-8} s	5.56×10^{-2} s	3.50×10^{-7} s

TABLE 2. Characteristic times evaluated at the end of the pulse ($\tau_{pulse} = 2$ ns) when the electron density is approximatley 2.2×10^{14} cm^{-3}.

3. Results

In this section, we report the results obtained by applying the model to different discharge and post-discharge conditions. In particular, two different initial discharge conditions have been selected considering applied reduced field E/N and pulse durations τ_{pulse} values of 200 Td, 2 ns and 130 Td 50 ns with different post-discharge times in the ms regime. On the other hand, pressure (1 atm) and gas temperature ($T_{gas} = 500$ K) are kept constant in all the numerical examples. The selected examples are sufficient to understand the non-equilibrium effects in both EEDF and VDF.

3.1. *Case study 1*

The following initial conditions are selected $T_{gas} = 500$ K, $p = 1$ atm, E/N = 200 Td, $\tau_{pulse} = 2$ ns, $\tau_{afterglow} = 10$ ms. Before examining the results, we want to anticipate that these E/N and τ_{pulse} values minimize the input of vibrational quanta in the CO molecule, i.e. the increase of the corresponding macroscopic vibrational temperature of CO (T_{v-CO}) is expected to be very small. On the other hand, the EEDF in the discharge will reach a quasistationary condition in times much less than the pulse duration.

We expect a minor role of vibrational superelastic collisions in the EEDF due to the corresponding low vibrational temperature. In addition, during the discharge, the superelastic electronic collisions should have a limited effect on the EEDF because the high electron temperature controlled by the high E/N value is such to hide the peaks formed by these collisions, the reverse will be in post-discharge conditions.

These observations are confirmed by inspection of the typical relaxation times for the present condition reported in the following table (table 2), which represent, in order, the time to achieve a quasistationary EEDF (τ_{EEDF}), the characteristic time to pump the vibrational energy in the system (τ_{e-V}), the time of V–V energy-exchange processes (τ_{V-V}) and the time of V–T relaxation by CO ($\tau_{V-T(CO)}$) and by C and O ($\tau_{V-T(C,O)}$). Such relaxation times are calculated from the corresponding rates linking the ground and the first vibrational level.

From table 2, we can see that $\tau_{e-V} > \tau_{pulse}$ implying a very small vibrational pumping in the system. This is indeed the case as can be observed from figure 2(*a*), where the 0–1 vibrational temperature of CO and the electron temperature are reported as a function of time in the discharge and post-discharge conditions.

We observe that the vibrational temperature of CO presents a very small increase from 500 to 640 K, while the electron temperature soon reaches a quasistationary value of approximately 30 000 K, in the so-called cold gas approximation. In this case, under discharge conditions, superelastic vibrational collisions are practically absent, while superelastic electronic collisions are hidden by the heating of EEDF by the applied E/N value, as already anticipated. In the post-discharge conditions, we can observe an abrupt decrease of electron temperature following the turning off of the

https://doi.org/10.1017/S0022377817000952 Published online by Cambridge University Press

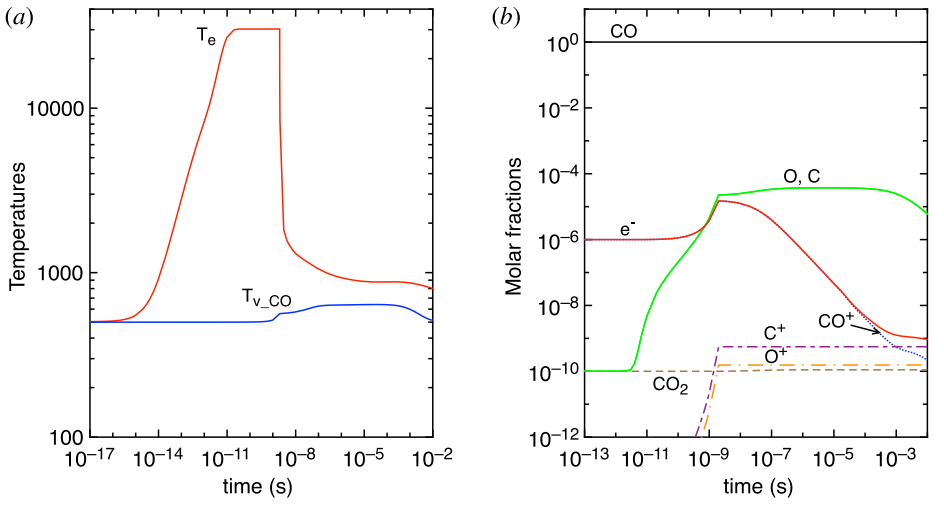

FIGURE 2. (*a*) Temperature and (*b*) molar fraction time evolution in case study 1 ($T_{gas} = 500$ K, $p = 1$ atm, E/N = 200 Td, $\tau_{pulse} = 2$ ns, $\tau_{afterglow} = 10$ ms).

electric field. Figure 2(*b*), on the other hand, reports the concentration of the different species under discharge and post-discharge conditions. We can observe an increase of approximately an order of magnitude in the electron density under discharge conditions, followed by its rapid decrease in the post-discharge due to the dissociative recombination process with CO^+. Carbon and oxygen atom concentrations formed under discharge conditions by direct electron-impact collisions keep their values in the post-discharge up to 10 ms, starting to decrease for $t > 10$ ms as a result of the recombination process (2.1.8). C^+ and O^+ species start being relatively important in the post-discharge for $t > 1$ ms.

The vibrational distribution for this case study is reported in figure 3 as a function of time in (*a*) discharge and (*b*) post-discharge conditions. Under discharge conditions, the VDF is controlled by e–V transition over the whole vibrational ladder, i.e. by the process $e–V_{Res}$ in table 1. The corresponding rates decrease with increasing v_f generating the form reported in figure 3(*a*). Once the VDF tail is sufficiently pumped by e–V processes, for $t > 10$ ns, only a small depletion of the VDF tail for $v > 60$ is observed due to the effect of the direct dissociation process (2.1.1), while the contribution of the Boudouard process, which acts in an intermediate range of v values ($v > 20$), is hidden by the dominance of e–V processes.

During the post-discharge, see figure 3(*b*), the quanta introduced by e–V processes are, to a given extent, redistributed by V–V processes and then deactivated by V–T ones. In any case, the corresponding plateaux present a molar fraction of 10^{-7}, insufficient to activate pure vibrational mechanisms in the dissociation process.

Figure 4 presents the corresponding time dependent EEDF. Under discharge conditions (figure 4*a*) the EEDF rapidly reaches a quasistationary condition characterized by a quasi-Maxwellian distribution function. More interesting is the behaviour of the EEDF post-discharge, which is governed by the repetition of different peaks due to the superelastic electronic collisions of CO metastables and cold electrons, confirming the parametric study of Gorse *et al.* (1986). In the present study, the concentration of CO electronically excited states is calculated as a result of pumping and deactivation by electron-impact collisions (see Met_{CO} processes in table 1), disregarding optical

https://doi.org/10.1017/S0022377817000952 Published online by Cambridge University Press

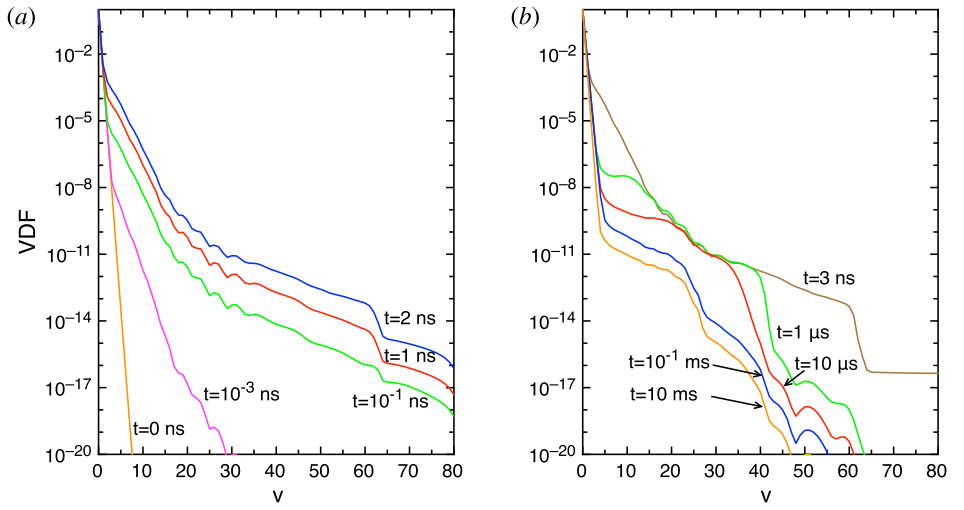

FIGURE 3. Vibrational distribution function in (*a*) discharge and (*b*) post-discharge conditions for case study 1 ($T_{gas} = 500$ K, $p = 1$ atm, E/N = 200 Td, $\tau_{pulse} = 2$ ns, $\tau_{afterglow} =$ 10 ms).

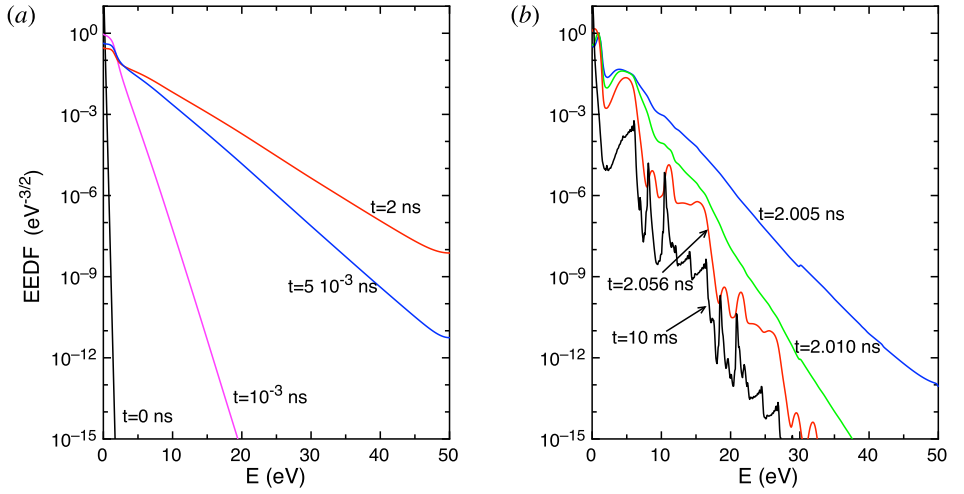

FIGURE 4. Electron energy distribution function in (*a*) discharge and (*b*) post-discharge conditions for case study 1 ($T_{gas} = 500$ K, $p = 1$ atm, E/N = 200 Td, $\tau_{pulse} = 2$ ns, $\tau_{afterglow} =$ 10 ms).

and quenching processes. The peaks reported in figure 4(*b*) reflect the threshold energies of the CO electronically excited states considered in the present work, which are more numerous than the choice of Gorse *et al.* (1986). It should be noted that the role of electronic states becomes evident when the reduced electric field is turned off, determining a very cold EEDF in the low energy zone, thus allowing to the considered excited states to manifest the role of superelastic electronic collisions in forming repetitive structures in the EEDF. In addition, the numerous CO electronic

https://doi.org/10.1017/S0022377817000952 Published online by Cambridge University Press

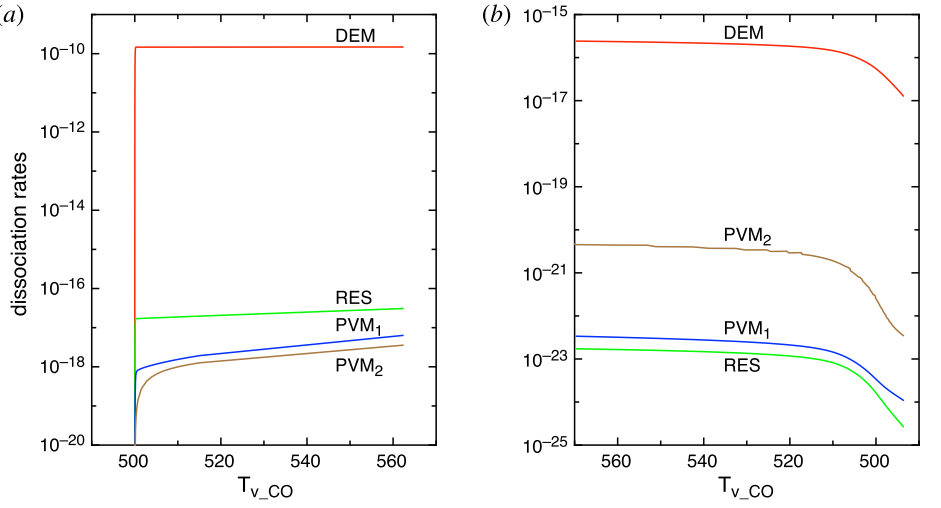

FIGURE 5. Dissociation rates ($cm^3\ s^{-1}$) as a function of the vibrational temperature in (*a*) discharge and (*b*) post-discharge conditions for case study 1 ($T_{gas} = 500$ K, $p = 1$ atm, E/N = 200 Td, $\tau_{pulse} = 2$ ns, $\tau_{afterglow} = 10$ ms).

excited states inserted in the Boltzmann equation form a quasicontinuous sequence of maxima in the EEDF.

In figure 5, we report the CO dissociation rates due to the different reactive channels as a function of the vibrational temperature in (*a*) discharge and (*b*) post-discharge conditions. In particular, we report the rate of the direct electron impact dissociation process DEM (see process in (2.1.3)), resonant dissociation process (RES) (see process D_{Res} in table 1) and pure vibrational mechanisms of direct dissociation PVM_1 (see process in (2.1.1)) and Boudouard process PVM_2 (see process in (2.1.2)). The explicit rate expressions can be found in Pietanza *et al.* (2017*b*) (see also the appendix A). As we can note, the plasma kinetics is dominated by direct dissociation electron-impact mechanisms, since the corresponding DEM rates are larger than the PVM_1 and PVM_2 ones, the difference decreasing in the post-discharge.

3.2. *Case study 2*

The selected conditions change in E/N = 130 Td and $\tau_{pulse} = 50$ ns, implying a larger vibrational energy pumping as compared with the previous case. The relevant results qualitatively follow those reported in the previous case, as can be observed by looking at the corresponding figures (see figures 6–9). In this case, however, the vibrational temperature of CO increases up to 1400 K (see figure 6*a*), enhancing the electron temperature at the end of the pulse as a consequence of superelastic vibrational collisions (see the peak in T_e at the end of the pulse). The trend of the electron and C and O molar fractions follow the previous ones also from a quantitative point of view (compare figures 6*b* and 2*b*). Their molar fractions reach a value of 10^{-4} against 10^{-5} obtained in the first case, the pulse duration being more important than the choice of E/N value in increasing the molar fraction of C and O atoms. The electron molar densities are very similar in the two cases because a sort of compensation exists between E/N value and pulse duration for the two case studies, i.e. the increase of ionization rates with E/N in case 1 is compensated for by the increase of rates due to the increase of the pulse duration in case 2.

https://doi.org/10.1017/S0022377817000952 Published online by Cambridge University Press

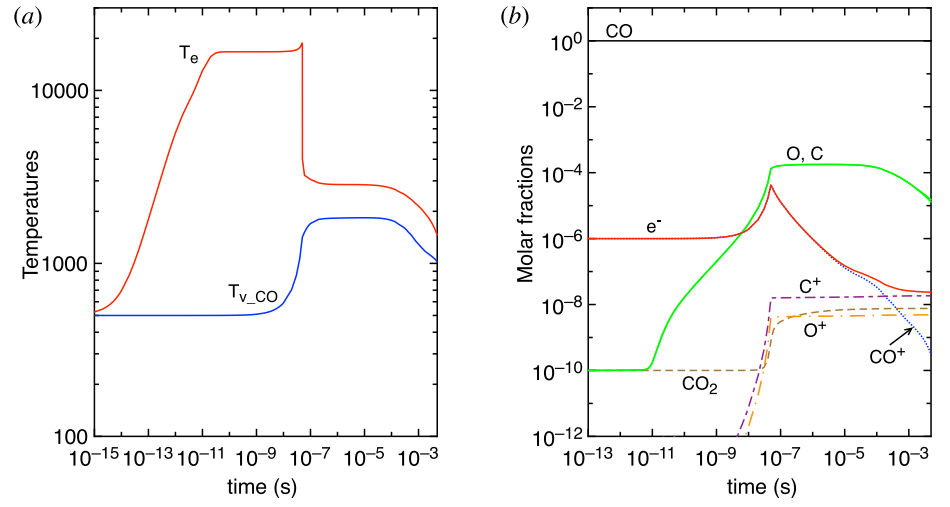

FIGURE 6. (*a*) Temperature and (*b*) molar fraction time evolution in case study 2 (T_{gas} = 500 K, p = 1 atm, E/N = 130 Td, τ_{pulse} = 50 ns, $\tau_{afterglow}$ = 4 ms).

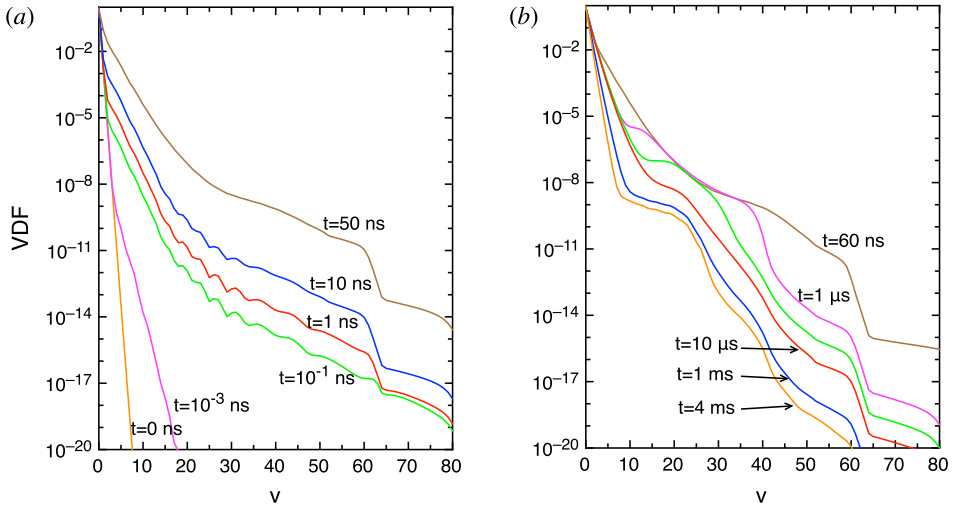

FIGURE 7. Vibrational distribution function in (*a*) discharge and (*b*) post-discharge conditions for the case study 2 (T_{gas} = 500 K, p = 1 atm, E/N = 130 Td, τ_{pulse} = 50 ns, $\tau_{afterglow}$ = 4 ms).

The characteristic times reported in table 3 for this case study are very similar to those reported for case study 1 (table 2), the major difference being the increase of vibrational temperature in this case as well as the higher production of C and O atoms due to the long pulse duration.

Qualitatively, the time evolution of the VDF under discharge and post-discharge conditions is similar to the results of previous case even though quantitatively the VDF, in the new case, is orders of magnitude higher than the 2 ns/200 Td case, both in discharge and post-discharge conditions, i.e. the pulse duration is more effective than E/N in increasing the input of vibrational quanta in the vibrational ladder. The reverse is observed for EEDF in both discharge and post-discharge conditions. In both cases, the EEDF at 200 Td is more populated than the corresponding values at

https://doi.org/10.1017/S0022377817000952 Published online by Cambridge University Press

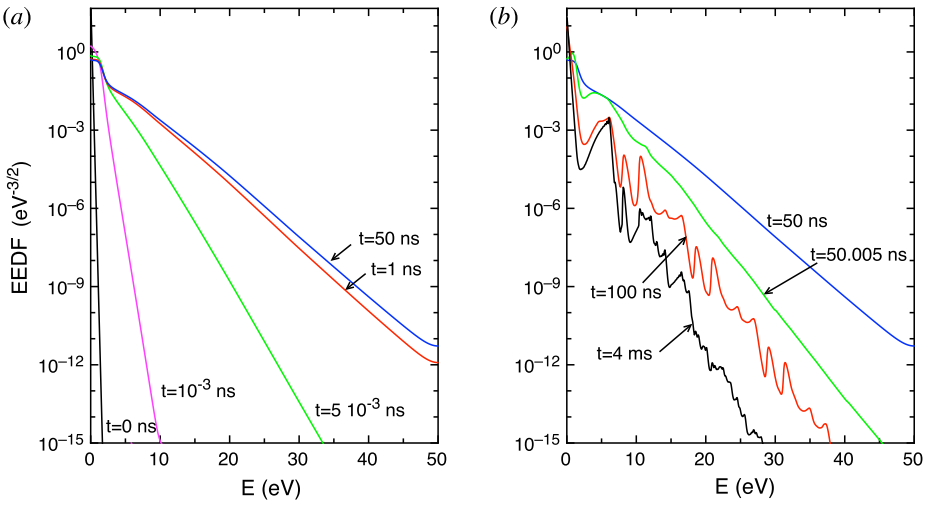

FIGURE 8. Electron energy distribution function in (*a*) discharge and (*b*) post-discharge conditions for case study 1 (T_{gas} = 500 K, p = 1 atm, E/N = 130 Td, τ_{pulse} = 50 ns, $\tau_{afterglow}$ = 4 ms).

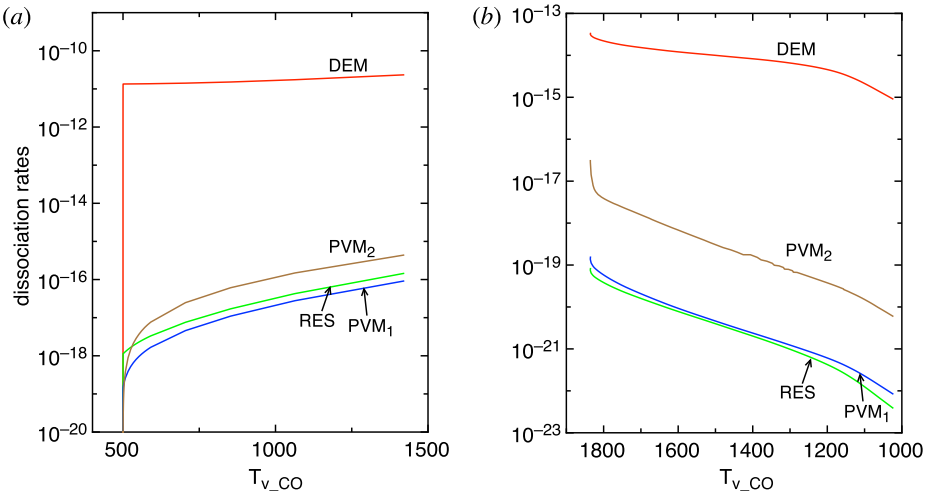

FIGURE 9. Dissociation rates (cm^3 s^{-1}) as a function of the vibrational temperature in (*a*) discharge and (*b*) post-discharge conditions for case study 2 (T_{gas} = 500 K, p = 1 atm, E/N = 130 Td, τ_{pulse} = 50 ns, $\tau_{afterglow}$ = 4 ms).

τ_{EEDF}	τ_{e-V}	τ_{V-V}	$\tau_{V-T(CO)}$	$\tau_{V-T(C,O)}$
5.57×10^{-12} s	1.30×10^{-7} s	4.37×10^{-8} s	5.56×10^{-2} s	3.50×10^{-7} s

TABLE 3. Characteristic times evaluated at the end of the pulse (τ_{pulse} = 50 ns) when the electron density is approximately 2×10^{15} cm^{-3}.

https://doi.org/10.1017/S0022377817000952 Published online by Cambridge University Press

130 Td, i.e. the reduced electric field is predominant in forming the EEDF, the pulse duration is not active enough in the pumping of the electronically excited states. As a result, the EEDF in the post-discharge regime is more populated than in the first case study.

Finally, by looking to figure 9, where the dissociation rates are reported for this second case study, it is clear that PVM rates, in particular the one corresponding to the Boudouard process (PVM_2), are increased with respect to case study 1, due to the higher vibrational excitation, which start approaching the DEM rates. Also in this case, the DEM rates remain higher that the PVM ones.

4. Conclusions and perspectives

The present results indicate the importance of the pulse duration in increasing the population of vibrational excited states and their role in affecting the PVM mechanisms in the activation of CO. In the 2 ns/200 Td discharge conditions, we observe that the plasma chemistry is governed by the electron-impact processes. In addition, the population of electronically excited states becomes essential in shaping the EEDF in the post-discharge. This last behaviour is also present in the post-discharge of a 50 ns/130 Td pulse discharge; in this case, however, PVM rates start to approach the DEM ones. This behaviour becomes essential in the microwave discharges, as shown in Pietanza *et al.* (2017*b*).

The reported results can be used as a guide to choose the initial conditions in nanopulsed repetitive discharges, in particular the duration of each pulse and the time between the different pulses.

An interesting aspect of the results presented in figures 2–5 is their qualitative and quantitative similarity with the corresponding ones reported by Capitelli *et al.* (2017*a*) for the same conditions as case 1 in CO_2 discharge and post-discharge conditions. In the CO_2 case, the molar fraction and VDF of CO_2 present a time dependent behaviour similar to that of CO, shown in the present case study 1. This can be observed by comparing the results of figures 2–5 of the present paper and the corresponding figures 9–12 in Capitelli *et al.* (2017*a*). The similarity in the trends emphasizes the necessity of considering vibrational excitation of CO with the same accuracy as that of CO_2, in the context of the CO_2 plasma activation problem. In the post-discharge of the CO system (figure 4*b*), we observe a more structured EEDF than in the CO_2 case (see figure 11*b* in Capitelli *et al.* 2017*a*), which could have some role in the global kinetics of CO_2. Of course, the introduction of the whole CO vibrational kinetics in the corresponding one for CO_2 increases the computational time especially for higher-dimensional model (one, two and three dimensions).

An alternative could be to use reduction approaches to simplify the global kinetics, as recently proposed by Colonna *et al.* (2006) for the activation of diatomic molecules, based on the kinetics of the last vibrational bound state. This model could be applied when the so-called ladder climbing model (Capitelli, Dilonardo & Molinari 1977; Capitelli, Colonna & Esposito 2004) can be used for describing the dissociation of the molecule, as also reported (to a given extent) in the CO_2 case by Peeremboom, Khaj & Degrez (2017).

In the case of CO, this model cannot be applied because the last bound level is scarcely populated and the PVM_2 mechanism needs the opening of a reaction involving an intermediate level, this situation being present under many situations of cold plasmas (see for example Colonna *et al.* 1999). This means that the reduction theory of Colonna *et al.* (2006) should be refined to introduce a series of levels which typically mime the opening of reactive channels.

https://doi.org/10.1017/S0022377817000952 Published online by Cambridge University Press

The other conclusion of the present paper is the role of the metastable electronic states of CO in forming structures in EEDF, as a consequence of the superelastic collisions of these states with cold electrons. We can anticipate that these processes will occur also in the CO_2 mixture producing CO with large consequences on the corresponding EEDF and more in general on the plasma kinetics. As a perspective, we will introduce a more robust kinetics for these metastable states. In the present approach, the population and depopulation of excited states are due to electron collisions, neglecting optical decay and quenching reactions. Taking these reactions into account (see for example Colonna & Capitelli 2001; Colonna *et al.* 2017*b*), including the redistribution of electronic energy after the quenching process (Pietanza *et al.* 2017*b*), will probably introduce a new scenario in the form of EEDF and VDF in the post-discharge. In this context, the models developed for describing CO shock wave flow should be also taken into account (Aliat, Chikhaoui & Kustova 2003, 2005). In addition, the theoretical dissociative–recombination rates of process (2.1.9) by Mezei *et al.* (2015), including the calculated branching ratios to the formed electronically excited states of C and O atoms, should be considered. The relevant cross-sections and rates depend on the initial vibrational state of the CO^+ ions adding new complexity to the whole kinetics at the moment beyond the aim of the present work.

Finally, the present results can be also considered to be a possible guide for the understanding of the behaviour of DBD discharges, which present more complicated spatio-temporal profiles of E/N (see for example Levko, Paschulli & Raja 2017). In particular, the time dependent streamers are characterized by duration times ranging from the sub-nanosecond to several nano-second level and an electron density of 10^{14}–10^{15} cm^{-3}. Under these conditions, not too far from those reported in cases 1 and 2, we can expect a minor importance of the vibrational kinetics in affecting the EEDF especially for sub-nanosecond streamers. On the contrary, in both regimes, the EEDF keeps a memory of the electronic excited states, especially in the spatial zone characterized by a low reduced electric field.

Acknowledgement

This work is dedicated to Professor F. Pegoraro for his important contributions to the physics of collisionless plasmas.

Appendix A

The direct electron-impact dissociation rate (DEM) and the resonant dissociation rate (RES) are calculated by taking into account the contribution to dissociation from all the CO vibrational levels v, according to

$$\mathrm{DEM} = \sum_v k_D^{\mathrm{dir}}(v)(E/N, f_v, x_{E_i}, x_e, x_{\mathrm{C}}, x_{\mathrm{O}}, x_{\mathrm{C}^+}, x_{\mathrm{O}^+})f_v \tag{A 1}$$

$$\mathrm{RES} = \sum_v k_D^{\mathrm{Res}}(v)(E/N, f_v, x_{E_i}, x_e, x_{\mathrm{C}}, x_{\mathrm{O}}, x_{\mathrm{C}^+}, x_{\mathrm{O}^+})f_v, \tag{A 2}$$

where f_v is the molar fraction of the vth vibrational level and $k_D^{\mathrm{dir}}(v)$ and $k_D^{\mathrm{Res}}(v)$ are the rates for direct and resonant dissociation from the v level (i.e. the rates of processes $\mathrm{D_{dir}}$(v) and $\mathrm{D_{Res}}$(v) in table 1). $k_D^{\mathrm{dir}}(v)$ and $k_D^{\mathrm{Res}}(v)$ are calculated from the EEDF and the corresponding cross-sections by using (2.1.7) and thus depend indirectly

https://doi.org/10.1017/S0022377817000952 Published online by Cambridge University Press

also on E/N, f_v and x_{E_i}, x_e, x_C, x_O, x_{C^+}, x_{O^+}, which are, respectively, the molar fractions of CO electronic excited states, electrons, C, O, C^+ and O^+.

The two PVM rates for direct dissociation and Boudouard process can be calculated by

$$\mathrm{PVM}_1 = \frac{n_{\mathrm{CO}}}{n_e} \sum_v k_D^{\mathrm{direct}}(v)(\alpha, T_{\mathrm{gas}}) f_v \tag{A 3}$$

$$\mathrm{PVM}_2 = \frac{n_{\mathrm{CO}}}{n_e} \sum_{v,w} k_D^{\mathrm{Boud}}(v, w)(E_a, T_{\mathrm{gas}}) f_v f_w, \tag{A 4}$$

where $k_D^{\mathrm{direct}}(v)$ and $k_D^{\mathrm{Boud}}(v, w)$ are the rate of processes (2.1.1) and (2.1.2).

$k_D^{\mathrm{direct}}(v)$ is calculated from the corresponding rate from the ground state $k_D^{\mathrm{direct}}(0)$, taken from Macdonald *et al.* (2016), by applying the Fridman–Macheret α-model (see Fridman 2008), i.e.

$$k_D^{\mathrm{direct}}(v) = k_D^{\mathrm{direct}}(0) \exp(\alpha E_v / T_{\mathrm{gas}}), \tag{A 5}$$

where α (assumed equal to 1, as for strongly endothermic reactions) is a parameter that determines the efficiency of vibrational energy in lowering the reaction barrier of the ground state dissociation process. $k_D^{\mathrm{Boud}}(v, w)$, instead, is calculated from Essenhigh *et al.* (2006), strongly depending on the chosen activation energy E_a value.

REFERENCES

Aliat, A., Chikhaoui, A. & Kustova, E. V. 2003 Non equilibrium kinetics of a radiative CO flow behind a shock wave. *Phys. Rev.* E **68**, 056306.

Aliat, A., Chikhaoui, A. & Kustova, E. V. 2005 State to state reaction rates in gases with vibration-electronic-dissociation coupling: the influence on a radiative shock heated CO flow. *Chem. Phys.* **314**, 37–47.

Barreto, P. R., De O. Euclides, H., Albernaz, A. F., Aquilanti, V., Capitelli, M., Grossi, G., Lombardi, A., Macheret, S. & Palazzetti, F. 2017 Gas phase Boudouard reactions involving singlet–singlet and singlet triplet CO vibrationally excited states: implications for the non-equilibrium vibrational kinetics of CO/CO_2 plasmas. *Eur. Phys. J* D **71**, 259.

Belov, I., Vanneste, J., Aghaee, M., Paulussen, S. & Bogaerts, A. 2017 Synthesis of micro- and nanomaterials in CO_2 and CO dielectric barrier discharges. *Plasma Process. Polym.* **14** (3), 1600065.

Bogaerts, A., Wang, W., Berthelot, A. & Guerra, V. 2016 Modeling plasma-based CO_2 conversion: crucial role of the dissociation cross section. *Plasma Sources Sci. Technol.* **25**, 055016.

Cacciatore, M., Capitelli, M., De Benedictis, S., Dilonardo, M. & Gorse, C. 1986 Vibrational kinetics, dissociation and ionization of diatomic molecules under non equilibrium conditions. *Topics Curr. Phys.* **39**, 5–46.

Capitelli, M., Celiberto, R., Colonna, G., Esposito, F., Gorse, C., Hassouni, K., Laricchiuta, A. & Longo, S. 2016 *Fundamental Aspects of Plasma Chemical Physics, Kinetics*, Springer Series on Atomic, Optical and Plasma Physics. Springer.

Capitelli, M., Colonna, G., D'Ammando, G., Hassouni, K., Laricchiuta, A. & Pietanza, L. D. 2017*b* Coupling of plasma chemistry, vibrational kinetics, collisional-radiative models and electron energy distribution function under non-equilibrium conditions. *Plasma Process. Polym.* **14**, 1600109.

Capitelli, M., Colonna, G., D'Ammando, G. & Pietanza, L. D. 2017*a* Self-consistent time dependent vibrational and free electron kinetics for CO_2 dissociation and ionization in cold plasmas. *Plasma Sources Sci. Technol.* **26**, 055009.

https://doi.org/10.1017/S0022377817000952 Published online by Cambridge University Press

CAPITELLI, M., COLONNA, G. & ESPOSITO, F. 2004 On the coupling of vibrational relaxation with the dissociation–recombination kinetics: from dynamics to aerospace applications. *J. Phys. Chem.* A **108**, 8930–8934.

CAPITELLI, M., DILONARDO, M. & MOLINARI, E. 1977 A theoretical calculation of dissociation rates of molecular hydrogen in electric discharges. *Chem. Phys.* **20**, 417–429.

CAPITELLI, M., FERREIRA, C. M., GORDIETS, B. F. & OSIPOV, A. I. 2000 *Plasma Kinetics in Atmospheric Gases*, Springer Series on Atomic, Optical, and Plasma Physics. Springer.

COLONNA, G., ARMENISE, I., BRUNO, D. & CAPITELLI, M. 2006 Reduction of state-to-state kinetics to macroscopic models in hypersonic flows. *J. Thermophys. Heat Transfer* **20**, 477–486.

COLONNA, G. & CAPITELLI, M. 2001 The influence of atomic and molecular metastable states in high-enthalpy nozzle expansion nitrogen flows. *J. Phys.* D*: Appl. Phys.* **34**, 1812–1818.

COLONNA, G., D'AMMANDO, G. & PIETANZA, L. D. 2017*a* The role of molecular vibration in nanosecond repetitively pulsed discharges and in DBDs in hydrogen plasmas. *Plasma Sources Sci. Technol.* **25** (5), 054001.

COLONNA, G., LAPORTA, V., CELIBERTO, R., CAPITELLI, M. & TENNISON, J. 2015 Non-equilibrium vibrational and electron energy distributions functions in atmospheric nitrogen ns pulsed discharges and ms post-discharges: the role of electron molecule vibrational excitation scaling-laws. *Plasma Sources Sci. Technol.* **24**, 035004.

COLONNA, G., PIETANZA, L. D., D'AMMANDO, G., CELIBERTO, R., CAPITELLI, M. & LARICCHIUTA, A. 2017*b* Vibrational kinetics of electronically excited states in H_2 discharges. *Eur. Phys. J* D **71**, 279.

COLONNA, G., TUTTAFESTA, M., CAPITELLI, M. & GIORDANO, D. 1999 Non-Arrhenius NO formation rate in one dimensional nozzle air flow. *J. Thermophys. Heat Transfer* **13**, 372–375.

COSBY, P. C. 1993 Electron-impact dissociation of carbon monoxide. *J. Chem. Phys.* **98**, 7804.

ESSENHIGH, K. A., UTKIN, Y. G., BERNARD, C., ADAMOVICH, I. V. & RICH, J. W. 2006 Gas-phase Boudouard disproportionation reaction between highly vibrationally excited CO molecules. *Chem. Phys.* **330**, 506–514.

FRIDMAN, A. 2008 *Plasma Chemistry*. Cambridge University Press.

GORSE, C., CACCIATORE, M. & CAPITELLI, M. 1984*a* Kinetic processes in non-equilibrium carbon monoxide discharges. I Vibrational kinetics and dissociation rates. *Chem. Phys.* **85**, 165–176.

GORSE, C. & CAPITELLI, M. 1984*b* Kinetic processes in non-equilibrium carbon monoxide discharges. II Self-consistent electron energy distribution functions. *Chem. Phys.* **85**, 177–187.

GORSE, C., PANICCIA, F., BRETAGNE, J. & CAPITELLI, M. 1986 Electron energy distribution functions in Carbon Monoxide discharge and post-discharge conditions: the role of superelastic electronic collisions from $CO(A^3\Pi)$ state. *J. Appl. Phys.* **59**, 731–735.

ITIKAWA, Y. 2015 Cross sections for electron collisions with carbon monoxide. *J. Phys. Chem. Ref. Data* **44**, 013105; Itikawa database, www.lxcat.net.

KOSAREVA, A. A. & NAGNIBEDA, E. A. 2017 Vibrational-chemical coupling in mixtures CO_2/CO/O and CO_2/CO/O_2/O/C. *J. Phys.: Conf. Ser.* **815**, 012027.

KOZAK, T. & BOGAERTS, A. 2014 Splitting of CO_2 by vibrational excitation in non-equilibrium plasmas: a reaction kinetics model. *Plasma Sources Sci. Technol.* **23**, 045004.

KOZAK, T. & BOGAERTS, A. 2015 Evaluation of the energy efficiency of CO_2 conversion in microwave discharges using a reaction kinetics model. *Plasma Sources Sci. Technol.* **24**, 015024.

LAHER, R. R. & GILMOR, F. R. 2016 Updated excitation and ionization cross sections for electron impact on atomic oxygen. *J. Phys. Chem. Ref. Data* **19**, 277.

LAPORTA, V., CASSIDY, C. M., TENNYSON, J. & CELIBERTO, R. 2012 Electron-impact resonant vibration excitation cross sections and rate coefficients for carbon monoxide. *Plasma Sources Sci. Technol.* **21**, 045005.

LAPORTA, V., TENNYSON, J. & CELIBERTO, R. 2016 Carbon monoxide dissociative attachment and resonant dissociation by electron-impact. *Plasma Sources Sci. Technol.* **25**, 01LT04.

LEVKO, D., PASCHULLI, M. & RAJA, M. L. 2017 Particle in cell modeling of shear branching in CO_2 gas. *J. Phys.* D*: Appl. Phys.* **50**, 354004.

MACDONALD, R. L., MUNAFO', A., JOHNSTON, C. O. & PANESI, M. 2016 Nonequilibrium radiation and dissociation of CO molecules in shock-heated flows. *Phys. Rev. Fluids* **1**, 043401.

MEZEI, J. ZS., BACKODISSA-KIMINOU, R. D., TUDORACHE, D. E., MOREL, V., CHAKRABARTI, K., MOTAPON, O., DULIEU, O., ROBERT, J., TCHANG-BRILLET, W.-U., BULTEL, A. *et al.* 2015 Dissociative recombination and vibrational excitation of CO^+: model calculations and comparison with experiments. *Plasma Sources Sci. Technol.* **24**, 035005.

MISHINA, A. I. & KUSTOVA, E. V. 2017 Spatially homogeneous relaxation of CO molecules with resonant VE transitions. *Vestn. St. Peterburg Univ.: Math.* **50**, 188–197.

MORI, S. & SUZUKI, M. 2009 Characterization of carbon nanofibers synthesized by microwave plasma-enhanced CVD at low-temperature in a $CO/Ar/O_2$ system. *Diam. Relat. Mater.* **18**, 678.

NIST Atomic Spectra Database at https://www.nist.gov/pml/atomic-spectra-database.

PEEREMBOOM, K., KHAJ, M. & DEGREZ, G. 2017 Pooling through cooling: creating optimal vibrational non-equilibrium CO_2 by supersonic expansion. *J. Phys.* D*: Appl. Phys.* **50**, 195201.

PIETANZA, L. D., COLONNA, G. & CAPITELLI, M. 2017*b* Non-equilibrium plasma kinetics of reacting CO: an improved state to state approach. *Plasma Sources Sci. Technol.* **26**, 125007.

PIETANZA, L. D., COLONNA, G., D'AMMANDO, G. & CAPITELLI, M. 2017*a* Time-dependent coupling of electron energy distribution function, vibrational kinetics of the asymmetric mode of CO_2 and dissociation, ionization and electronic excitation kinetics under discharge and post-discharge conditions. *Plasma Phys. Control. Fusion* **59**, 014035.

PIETANZA, L. D., COLONNA, G., D'AMMANDO, G. & CAPITELLI, M. 2017*c* Time-dependent coupling of electron energy distribution function, vibrational kinetics of the asymmetric mode of CO_2 and dissociation, ionization and electronic excitation kinetics under discharge and post-discharge conditions. *Plasma Phys. Control. Fusion* **59**, 014035.

PIETANZA, L. D., COLONNA, G., D'AMMANDO, G., LARICCHIUTA, A. & CAPITELLI, M. 2015 Vibrational excitation and dissociation mechanisms of CO_2 under non-equilibrium discharge and post-discharge conditions. *Plasma Sources Sci. Technol.* **24**, 042002.

PITCHFORD, L. C., ALVES, L. A., BARTSCHAT, K., BIAGI, S. F., BORDAGE, M. C., BRAY, I., BRION, C. E., BRUNGER, M. J., CAMPBELL, L., CHACHEREAU, A. *et al.* 2017 LXCat: an open-access, web-based platform for data needed for modeling low temperature plasmas. *Plasma Process. Polym.* **14**, 1600098.

ROCKWOOD, S. D. 1973 Elastic and inelastic cross sections for electron-Hg scattering from Hg transport data. *Phys. Rev.* A **8**, 2348–2358.

WANG, Y., ZATSARINNY, O. & BARTSCHAT, K. 2013 B-spline R-matrix-with-pseudostates calculations for electron-impact excitation and ionization of carbon. *Phys. Rev.* A **87**, 012704.

https://doi.org/10.1017/S0022377817000952 Published online by Cambridge University Press